MS-Based Metabolomics Reveals Metabolic Dysregulation in Erastin-Induced Gastric Adenocarcinoma Cells

Ying Liu
Zhengzhou University
Wenchao Hu
Zhengzhou University
Mogesdessale Asmamaw
Zhengzhou University
Lulu Pan
Zhengzhou University
Juan Li (jli@zzu.edu.cn)
Zhengzhou University
Hongmin Liu
Zhengzhou University

Research Article

Keywords: Metabolomics, Pseudotargeted method, LC-MS/MS, Erastin, MGC-803 cells, Gastric cancer

Posted Date: September 30th, 2021

DOI: https://doi.org/10.21203/rs.3.rs-927028/v1

Abstract

Gastric cancer (GC) is one of the most malignant tumors with high morbidity and mortality in the world, particularly in China. Erastin, a classical ferroptosis inducer, exerts cytotoxicity in several types of cancer cells including gastric cancer cells. However, the mechanism of erastin in regulating metabolic pathways in gastric cancer remains largely unclear. To investigate the gastric cellular response to erastin therapy, we adopted a cell pseudotargeted metabolomics method based on liquid chromatography-hybrid triple quadrupole linear ion trap mass spectrometry (LC-QTRAP MS). The developed method was used to investigate the differential metabolites between erastin-treated MGC-803 cells and the controls at different time points. We found that erastin induced tremendous impact on the metabolome of gastric cells by affecting key metabolic processes, such as cysteine and methionine metabolism, glutathione (GSH) biosynthesis, glycolysis and TCA cycle. Interestingly, S-adenosylmethionine (SAM), methionine, serine, glycine and cysteine were obviously increasing treads after erastin treatment, but S-adenosylhomocysteine (SAH) and GSH were always down-regulated up to 48 h. The results indicated that DNA methylation was activated and glutathione biosynthesis was blocked in erastin-treated MGC-803 gastric cells, highlighting the importance of erastin as a promising drug candidate for in *vivo* treatment of gastric tumor.

Introduction

Gastric cancer (GC) ranks fourth in incidence and third in mortality among all the cancers worldwide, and the high incidence rate occurs mainly in East Asia, East Europe, and South America[1,2]. Most cancers exhibit increased aerobic glycolysis, the Warburg effect, and oxidative stress, which can be exploited as an important therapeutic target in the development of new anticancer strategies[3,4]. Moreover, Cancer cells usually possess high level of ROS and high antioxidant activities. Due to this, cancer cells are unable to cope with additional oxidative stress and become vulnerable to ROS-mediated cellular damage. Therefore, anticancer strategies that selectively raise level of ROS in cancer cells will represent a useful tool to combat the disease.

Erastin is a ferroptosis inducer that blocks cystine uptake through inhibition of cystine/glutamate antiporter (system X_C^-) eliminating glutathione (GSH) production. This causes a deficiency in the antioxidant defense system of the cell ultimately creating a redox homeostasis imbalance in cells due to ROS accumulation[5,6]. Besides, erastin can restore mitochondrial metabolism of malignant tumor cells and antagonize the Warburg phenomenon through blocking the inhibitory effect of free tubulin on voltage-dependent anion channel[7]. Erastin can kill human tumor cells exclusively, rapidly and irreversibly, without affecting normal cells of the same genotype[8]. Therefore, erastin represents a novel pharmacological agent which may become a new anti-cancer drug through regulating metabolism. Recent reports on erastin focused only on the molecular mechanism by which it induces ferroptosis in cancers[9-11]. However, the mechanism of erastin in regulating metabolic pathways in gastric cancer remains largely unclear.

Liquid chromatography tandem mass spectrometry (LC-MS/MS) is one of the most powerful techniques to characterize the metabolome of cultured cells owing to high sensitivity, simple sample pretreatment, and wide coverage of metabolites. Currently, mass spectrometry (MS)-based metabolomics can usually provide nontargeted and targeted strategies, each having their own advantages and disadvantages[12,13]. The nontargeted metabolomics strategy is usually operated on high resolution mass spectrometry (HRMS) including Orbitrap and time-of-flight (TOF), which can provide highly accurate masses and cover as many metabolites as possible in biological samples. However, there are some deficiencies using the nontargeted method, such as poor reproducibility, narrow linear range and complex data preprocessing. The targeted metabolomics strategy is often performed on triple quadrupole mass spectrometry with multiple reaction monitoring (MRM) mode, which has high sensitivity, good linearity and good reproducibility. However, the coverage of targeted analyses is limited as it usually focuses on known metabolites. To compensate for the two methods, Xu et.al developed a so called pseudotargeted metabolomics based on mass spectrometry (MS) operated in the MRM mode[14-16], which combines the advantages of both targeted and nontargeted strategies. Recently, MS-based pseudotargeted metabolomics and its similar strategies have been widely applied to investigate endogenous metabolites in different biological matrices[17-19].

Metabolomics studies the variation of small molecule metabolites using advanced analytical platforms and bioinformatics, and it can be largly associated with phenotypic changes[20]. The interaction of drugs with cells affects metabolic changes, and leads to an increase or decrease in metabolite levels. Metabolomics has the potential to dicover new end point biomarkers of drug efficacy or drug toxicity[21]. There is mourting evidence that metabolomics can provide new insights into the mechanism of action of drug candidates, and help find important enzyme targets for these candidates. In this work, we developed the pseudotargeted strategies with wide coverage of metabolites and good reproducibility using ultra-high performance liquid chromatography-hybrid triple quadrupole linear ion trap mass spectrometry (UHPLC-QTRAP MS). The developed method was applied to explore changes in endogenous metabolites in gastric cancer cells following erastin treatment for the first time. Human gastric adenocarcinoma MGC-803 cells were exposed to erastin for up to 48 h, and erastin-induced variations of endogenous metabolites were monitored at different time points, especially in cysteine and methionine metabolism, glutathione (GSH) biosynthesis, glycolysis and TCA cycle. This work may contribute to a better understanding of erastin's mechanisms of action and pave the way for metabolites (*in vitro*) to be explored as in *vivo* markers of therapy response.

Results

Development of the Pseudotargeted Metabolomics Method. The pseudotargeted metabolomics method was proposed based on LC/MS system operated in the MRM mode. Metabolomics allows the analysis of as many metabolites as possible, it is impossible to obtain a standard for each metabolite. In this work, the ~500 MRM ion pairs for pseudotargeted analysis were acquired by some metabolite standards or published literatures [16–19, 22], the ~350 MRM ion pairs were selected for the quantitative MRM transition,

along with a second transition for identity confirmation. The mass spectometry parameters and retention time (RT) are summarized in supplementary Table S1. The coverage of detected metabolites using the developed pseudotargeted method is involved in amino acid metabolism, nucleotidemetabolism, glycolysis, tricarboxylic acid (TCA) cycle, etc.

A total of ~278 ion peaks were determined by the use of the above analytical method. Representative MRM chromatograms of cell samples in the positive and negative detection modes are shown in Figs. 1(A, B). The pseudotargeted method was validated for repeatability, inter- and intra-day precision. The within-day precision was evaluated on the same day by QC samples, 13.7, 35.3, 69.4 and 92.5 % of the peaks had the relative standard deviation (RSDs) below 5, 10, 15 and 25 %, respectively (Fig. 2(A)). The inter-day precision was evaluated for three consecutive days, where 15.1, 33.8, 62.2 and 90.3 % of the peaks showed the RSDs below 5, 10, 15 and 25 %, respectively (Fig. 2(B)). The QC samples were also used to evaluate the repeatability of the method, and one QC sample was inserted after every six test cells. 13.3, 36.7, 61.9 and 91.4 % of the peaks had the RSDs below 5, 10, 15 and 25 %, respectively (Fig. 2(C)). These results showed that the developed method were suitable for metabolomics analysis in complex cell matrices.

Multivariate Analysis of the Metabolite Profile. The developed method was used to investigate the differential metabolites between erastin-treated MGC-803 cells and the controls. In order to screen for the metabolic difference between the controls and treated cells at different time points (6 h, 12 h, 24 h and 48 h), multivariate analysis was applied to the corresponding spectra (n = 48). Firstly, PCA and OPLS-DA models were built to show the difference of metabolites between erastin-treated cells and the controls. The PCA-X score plots are shown in Fig. 3. As shown in Fig. 3, in the PCA-X score plot, erastin-treated cells were obviously separated from the controls at different time points. It can therefore be concluded that erastin induced a great metabolic disorder in MGC-803 cells. The OPLS-DA score plots are shown in Fig. S1.

Heatmap Visualization. To further study the relative levels of differential metabolites between erastin-treated cells and the controls, a hierarchical cluster analysis (HCA) was performed on MEV software. The metabolites screened for the heatmap analysis were based on the principles of Student's *t*-test *p*-value <0.05 and the variable importance in projection (VIP) value >1 in OPLS-DA. The heatmap visualization of these differential metabolites showed a great difference between erastin-treated cells and the controls, which is consistent with OPLS-DA results. As shown in Fig. 4(A), 19 differential metabolites were discovered between erastin-treated cells and the controls with two metabolites increased and 17 metabolites decreased in treated cells at 6 h. In Fig. 4(B), 34 differential metabolites were discovered between erastin-treated cells and the controls with 18 metabolites increased and 16 metabolites decreased in treated cells at12 h. In Fig. 4(C), 23 differential metabolites were discovered between erastin-treated cells and the controls with one metabolite decreased and 22 metabolites increased. In Fig. 4(D), 29 differential metabolites were discovered between erastin- treated cells and the controls with two metabolites decreased and 27 metabolites increased.

Integrated Pathway Analysis. To better understand the differences of metabolic disorders between the erastin- treated cells and the controls, an integrated pathway analysis was carried out. MetaMapp is an R based script whose outputs are well compatible with the open-source platform CytoScape [23]. It can be used to visualize metabolomics datasets that can conclude all identified compounds while maintaining the modular organization of metabolites in biochemical pathways [24]. The metabolic relation network was generated through MetaMapp and drew by CytoScape (Fig. 5). The red lines represent the relationship between the two metabolites contained in KEGG. The blue lines represent the relationship between the two metabolites without contained in KEGG, but the related metabolites had a similar chemical structure, judged by PubChem. The diameter was corrected with the fold change value and *t*-test *p* value. The raw data is shown in Table S2.

Of the differential metabolites ($p<0.05$), 21% (18/87) and 43% (56/129) were up-regulated in erastin-treated cells at 6 h and 12 h, respectively. With the prolongation of drug action time, the up-regulated metabolites gradually increased. More than 90% of the differential metabolites were up-regulated in treated cells at 24 h or 48 h. As shown in Fig. 5(A), most of differential metabolites showed a decreasing trend in treated cells at 6 h. The metabolites with fold change values >3 were N_6-methyladenosine, inosine, 6-O-methylguanosine, 1-methyladenosine, and carbamoyl phosphate. The metabolites with fold change values <0.3 were reduced glutathione, melatonin, dCMP, cyclic di-AMP and sorbose. As shown in Fig. 5(B), the metabolites with fold change values >3, including 5-methylthioadenosine, N_6-methyladenosine, S-adenosyl-L-methionine, carbamoyl phosphate, glucose 1-phosphate, adenine, inosine, 6-O-methylguanosine, uridine and guanosine were mainly incorporated in nucleotide metabolism and glycolysis. The metabolites with fold change values < 0.3 were S-adenosyl-L-homocysteine, reduced glutathione, oxidized glutathione, dCMP, and melatonin. As shown in Figs. 5(C)~(D), most of the differential metabolites were up-regulated including amino acid metabolism, nucleotide metabolism, glycolysis and TCA cycle. Only a few metabolites with fold change values <0.3, including reduced glutathione, oxidized glutathione, S-adenosyl-L-homocysteine were mainly involved in cysteine and methionine metabolism and glutathione metabolism.

Discussion

Metabolomics allows for a global assessment of a cellular state, integrating genetic regulation, activity of enzymes, and cellular environment [25]. The present study exploited new developments in MS-based pseudotargeted metabolomics to help unravel mechanism of the response of MGC-803 cells to erastin. Response trajectory analysis of the metabolites was shown in Fig. 6. Glutathione (GSH) is an important regulator of intracellular metabolism. It can activate a variety of enzymes including sulfhydrylase and coenzyme, so as to promote carbohydrate, fat and protein metabolism. Ferroptosis pathway is being considered as an alternative anticancer therapeutic strategy, and the chemoreagent erastin induces ferroptosis by blocking system Xc(-), which causes a cysteine shortage that depletes intracellular GSH [26, 27]. In this study, reduced glutathione (GSH) had a significant downward trend in erastin-treated MGC-803 cells from 6 h to 48 h. However, cysteine, glycine and glumarate had an obvious increasing trend

compared to the controls. The result indicated that the activity of γ-glutamyl cysteine synthetase was dysregulated and synthesis of glutathione could be blocked [28].

S-adenosylmethionine (SAM) is an important metabolite and can act as a nutrition, energy and stress sensor in *vivo* and in *vitro*, thus regulating autophagy [29]. SAM dysregulation is involved in the occurrence and development of various diseases. In this study, serine and glycine showed an increasing trend after erastin treatment from 6 h to 48 h, which can initiate the folate cycle to facilitate the generation of SAM in the methionine cycle [30]. In this study, methionine and SAM showed a significant increasing trend, and the ratio of SAM to SAH also displayed an increasing trend, which indicates an enhancement in methylation ability in erastin-treated cells [29].

With the prolongation of erastin action time, there were obviously significant alterations in the levels of energy metabolism in erastin-treated cells. Compared to the controls, glucose and glucose 6-phosphate had low concentration levels in the MGC-803 cells treated from 6 h to 12 h, and high concentration levels from 24 h to 48 h. Concentration of glucose can further affect GSH levels, which was consistent with the literatures [31, 32]. In tricarboxylic acid cycle (TCA) cycle, oxaloacetate, 2-oxoglutarate and succinate had a decreasing trend in the MGC-803 cells treated from 6 h to 12 h, and an increasing trend from 12 h to 48 h, which has direct or indirect relationship with iron metabolism, such as an auxiliary factor of various proteins in TCA cycle [33].

Conclusion

In our study, a MS-based, time-series metabolomics approach was used for the first time to explore metabolite changes in erastin-induced gastric cancer cells. Exposure of cells to erastin induced a significant metabolic changes at all time points. In MGC-803 cells, erastin treatment for 24h and 48h induced a great increase in the levels of energy metabolism, particularly in amino acids, nucleosides, glycolysis and TCA cycle. However, GSH and GSH/GSSG were down- regulated after erastin treatment at all time points indicating the impact of erastin on cellular antioxidative stores. Taken together, our results revealed that energy metabolism disturbance and oxidative damage were the important factors in the response of MGC-803 gastric cells to erastin, especially, in cysteine and methionine metabolism, glutathione (GSH) biosynthesis, glycolysis and TCA cycle, highlighting the importance of erastin as a promising candidate for in *vivo* monitoring of gastric tumor responsiveness to treatment.

Methods

Chemicals and reagents. Metabolite standards and erastin were purchased from Sigma-Aldrich (USA). HPLC- grade acetonitrile, methanol, acetic acid and ammonium acetate were purchased from J.T. Baker (Phillipsburg, NJ, USA). Ultrapure water was obtained by Milli-Q water- purification system (Millipore, Bedford, MA, USA). Culture medium, fetal bovine serum and trypsin were purchased from Gibco-BRL (U.K.). Phosphate buffered saline (PBS, pH 7.4) was supplied by EuroCloneS.p.a. (Italy).

Cell culture and treatment. The human gastric adenocarcinoma cell line MGC-803 was obtained from Shanghai Institute for Biological Sciences (Chinese Academy of Science, China). MGC-803 cells were grown in Dulbecco's modified Eagle medium (DMEM) supplemented with 10 % fetal bovine serum, 2 mM glutamine, penicillin (100 U/mL) and streptomycin (100 μg/mL) at 37°C in a humidified atmosphere under 5% CO_2. The cells were cultured in 60-mm dishes at a cell density of ~10^6 per dish. After growing for 24 h, the cells were treated with erastin at a final working concentration of 20 μM. The cell samples (both control and erastin-treated) were then collected at different time points (6 h, 12 h, 24 h and 48 h).

The test cells were gently washed with PBS, and quickly frozen with liquid nitrogen (N_2) for metabolic quenching. Pretreatment procedure of the cells was applied according to our previous studies[22]. Briefly, methanol/acetonitrile/water (40/40/20, *v/v/v*) was added to cell dishes, the cell/solvent mixture were collected and transferred to clean tubes. After freeze-thaw cycle treatment, the extracts were centrifuged and transferred to clean tubes to be evaporated to dryness. The dry extracts were dissolved in acetonitrile/H_2O (70/30, *v/v*) prior to the LC-MS analysis. The quality control (QC) sample was prepared by mixing an equal aliquot of exacts from the controls and erastin-treated cells. The QC samples were used to survey stability and reproducibility of the instrument during analysis process.

LC-MS/MS analysis. The experiments were performed on ultra high performance liquid chromatography (UHPLC, Shimadzu, Japan) system. Chromatographic analysis was carried out on a BEH amide (1.7 μm, 2.1 ×100 mm) column. Autosampler temperature and column temperature were set at 4℃and 40℃, respectively. The mobile phases were B (acetonitrile) and A (15 mM ammonium acetate, pH~3.0). The elution program was as follows: 85%-50% B (0-14 min), 50%-85% B (14-15 min), 85% B (15-21 min). The flow rate was 0.2 mL/min, and the volume of injection was 1 μL.

The QTRAP 4500 mass spectrometer (AB SCIEX, Singapore) was used to perform pseudotargeted analysis. The main MS parameters were as follows. The electrospray voltages were set at 5500 V for ESI+ mode and -4500 V for ESI- mode. The ion spray temperature was 500℃. The ion source GAS1, ion source GAS2 and curtain GAS were set at 50, 50 and 20 psi, respectively. The collision energy was set at "medium". The reconstituted supernatants were analyzed both in positive and negative ion modes. The QC sample ran 5 times before the analysis of test cells, then inserted every six cell samples to assess repeatability of the method.

Data processing and statistical Analysis. The areas of the ion peaks detected by LC-MS/MS were analyzed and integrated using MultiQuant 2.1 software. The adjusted peak table was imported into SIMCA 14.0 software (Umetrics, Sweden) to carry out principal component analysis (PCA) and orthogonal partial least squares-discriminant analysis (OPLS-DA) analysis. Student's *t*-test was achieved on SPSS statistical software (version 21.0), and *p*-value <0.05 was considered statistically significant. Heatmap analysis was performed with MultiExperiment- Viewer software (MEV, version 4.7.4), which compared the relative levels of differential metabolites. Pathway enrichment analysis was carried out on MetaboAnalyst Web site (http://www.metaboanalyst.ca). The pathway mapping was analyzed with MetaMapp and CytoScape.

Declarations

Acknowledgments

This work was supported by National Natural Science Foundation of China (Project No. 81430085 and No. 81773562 for H.-M.Liu); National Key Research Program of Proteins (No. 2016YFA0501800 for H.-M. Liu); Key Research Program of Henan Province (No.1611003110100 for H.-M. Liu).

Author Contributions

Hong-Min Liu and Juan Li have conceptualized the work and designed the experimental procedures. Ying Liu has supplied erastin-treated gastric cancer cells and the control cells. Juan Li have performed the experiments with LC-MS and data analysis. Ying Liu and Wen-Chao Hu have prepared cell samples. Juan Li, Ying Liu and Wenchao Hu have prepared the figures, the tables and the first draft. The article was revised, and further improved by Moges Dessale Asmamaw and Lu-Lu Pan. Ying Liu and Juan Li edited the final manuscript.

Competing Interests: The authors declare no competing interests.

References

1. Siegel, R. L., Miller, K. D. & Jemal, A. Cancer statistics. *A Cancer Journal for Clinicians*, **66**, 7–30 (2016).
2. Rawla, P. & Barsouk, A. Epidemiology of gastric cancer: Global trends, risk factors and prevention. *Przeglad Gastroenterologiczny*, **14**, 26–38 (2019).
3. Cairns, R. A., Harris, I. S. & Mak, T. W. Regulation of cancer cell metabolism. *Nature Reviews.Cancer*, **11**, 85–95 (2011).
4. Liu, X. *et al.* Cystine transporter regulation of pentose phosphate pathway dependency and disulfide stress exposes a targetable metabolic vulnerability in cancer. *Nature Cell Biology*, **22**, 476–486 (2020).
5. Xie, Y. *et al.* Ferroptosis: Process and function. *Cell Death and Differentiation*, **23**, 369–379 (2016).
6. Yang, W. S. *et al.* Regulation of ferroptotic cancer cell death by GPX4., **156**, 317–331 (2014).
7. Maldonado, E. N. *et al.* Voltage-dependent anionchannels modulate mitochondrial metabolism in cancer cells: Regulationby free tubulin and erastin. *Journal of Biological Chemistry*, **288**, 11920–11929 (2013).
8. Sato, M. *et al.* The ferroptosis inducer erastin irreversibly inhibits system Xc- and synergizes with cisplatinto increase cisplatin's cytotoxicity in cancer cells. *Sci. Rep*, **8**, 968 (2018).
9. Zhao, Y. C. *et al.* The Role of Erastin in Ferroptosis and Its Prospects in Cancer Therapy. *OncoTargets and Therapy*, **13**, 5429–5441 (2020).

10. Hao, S. H. *et al.* Cysteine dioxygenase1 mediates erastin-induced ferroptosis in human gastric cancer cells. *Neoplasia*, **19**, 1022–1032 (2017).
11. Niu, Y., Zhang, J. P., Tong, Y. L., Li, J. & Liu, B. Physcion 8-O-β-glucopyranoside induced ferroptosis via regulating miR-103a-3p/GLS2 axis in gastric cancer. *Life Science*, **237**, 116893 (2019).
12. Evans, C. R. *et al.* Untargeted LC-MS metabolomics of bronchoalveolar lavage fluid differentiates acute respiratory distress syndrome from health. *Journal of Proteome Research*, **13**, 640–649 (2014).
13. Abdel Rahma, A. M., Pawling, J., Ryczko, M., Caudy, A. A. & Dennis, J. W. Targeted metabolomics in cultured cells and tissues by mass spectrometry: method development and validation. *Anal. Chim. Acta*, **845**, 53–61 (2014).
14. Chen, S. *et al.* Pseudotargeted metabolomics method and its application in serum biomarker discovery for hepatocellular carcinoma based on ultra high-performance liquid chromatography/triple quadrupole mass spectrometry. *Anal. Chem*, **85**, 8326–8333 (2013).
15. Zhou, Y. *et al.* Discovery and validation of potential urinary biomarkers for bladder cancer diagnosis using a pseudotargeted GC-MS metabolomics method. *Oncotarget*, **8**, 20719–20728 (2017).
16. Zheng, F. J. *et al.* Development of a plasma pseudotargeted metabolomics method based on ultra-high-performance liquid chromatography-mass spectrometry. *Nature Protocols*, **15**, 2519–2537 (2020).
17. Wang, Y. *et al.* An improved pseudotargeted metabolomics approach using multiple ion monitoring with time-staggered ion lists based on ultra-high performance liquidchromatography/quadrupole time-of-flight mass spectrometry. *Anal. Chim. Acta*, **927**, 82–88 (2016).
18. Yan, Z. & Yan, R. Increase the accessibility and scale of targeted metabolomics: construction of a human urinary metabolome-wide multiple reaction monitoring library using directly-coupled reversed-phase and hydrophilic interaction chromatography. *Anal. Chim. Acta*, **894**, 65–75 (2015).
19. Wang, L. C. *et al.* Ion-pair selection method for pseudotargeted metabolomics based on SWATH MS acquisition and itsapplication in differential metabolite discovery of type 2 diabetes. *Anal. Chem*, **90**, 11401–11408 (2018).
20. Wang, Liu, Y. S., Hu, Y., Li, P. & Wan, J. B. Current state of the art of mass spectrometry-based metabolomics studies: a review focusing on widecoverage, high throughput and easy identification. *RSC Advances*, **5**, 78728–78737 (2015).
21. Robertson, D. G., Watkins, P. B. & Reily, M. D. Metabolomics in Toxicology: Preclinical and Clinical Applications. *Toxicol. Sci*, **120**, S146–S170 (2011).
22. Li, J. *et al.* Development of a mass spectrometry-based pseudotargeted metabolomics strategy to analyze hormone- stimulated gastric cancer cells. *Journal of Pharmaceutical and Biomedical Analysis*, **180**, 113041 (2020). **)**
23. Barupal, D. K. *et al.* Fiehn, O. MetaMapp: mapping and visualizing metabolomic data by integrating information from biochemical pathways and chemical and mass spectral similarity. *BMC bioinformatics*, **13**, 99 (2012).

24. Grapov, D., Wanichthanarak, K. & Fiehn, O. MetaMapR: pathway independent metabolomic network analysis incorporating unknowns., **31**, 2757–2760 (2015).
25. Daddiouaissa, D., Amid, A., Sani, M. S. A. & Elnour, A. A. M. Evaluation of metabolomics behavior of human colon cancer HT29 cell lines treated with ionic liquid graviola fruit pulp extract. *Journal of Ethnopharmacology*, **270**, 113813 (2021).
26. Kim, H., Lee, J. H. & Park, J. W. Down-regulation of IDH2 sensitizes cancer cells to erastin-induced ferroptosis, Biochemical and Biophysical Research Communications, 525,366–371(2020).
27. Sun, Y. W., Deng, R. R. & Zhang, C. W. Erastin induces apoptotic and ferroptotic cell death by inducing ROS accumulation by causing mitochondrialdysfunction in gastric cancer cell HGC-27. *Mol. Med. Rep*, **22**, 2826–2832 (2020).
28. Kennedy, L., Sandhu, J. K. & Harper, M. E. Miroslava Cuperlovic-Culf, Role of Glutathione in Cancer: From Mechanisms to Therapies. *Biomolecules*, **10**, 1429 (2020).
29. Ouyang, Y., Wu, Q., Li, J., Sun, S. & Sun, S. S-adenosylmethionine: A metabolite critical to the regulation of autophagy. *Cell Prolif*, **53**, e12891 (2020).
30. Wu, Q., Chen, X., Li, J. & Sun, S. Serine and metabolism regulation: a novel mechanism in antitumor immunity and senescence.Aging and Disease11, (2020).
31. Kumar, S. M., Swaminathan, K., Clemens, D. L. & Dey, A. GSH protects against oxidative stress and toxicity in VL-17A cells exposed to high glucose. *European Journal of Nutrition*, **54**, 223–234 (2015).
32. Achari, A. E. & Jain, S. K. L-Cysteine supplementation increases insulin sensitivity mediated by upregulation of GSH and adiponectin in high glucose treated 3T3-L1 adipocytes. *Archives of Biochemistry and Biophysics*, **630**, 5465 (2017).
33. Kashlov, Y. & Dimova, M. Ferroptosis and its potential role in cardiovascular diseases. *Journal of IMAB*, **25**, 2414–2418 (2019).

Figures

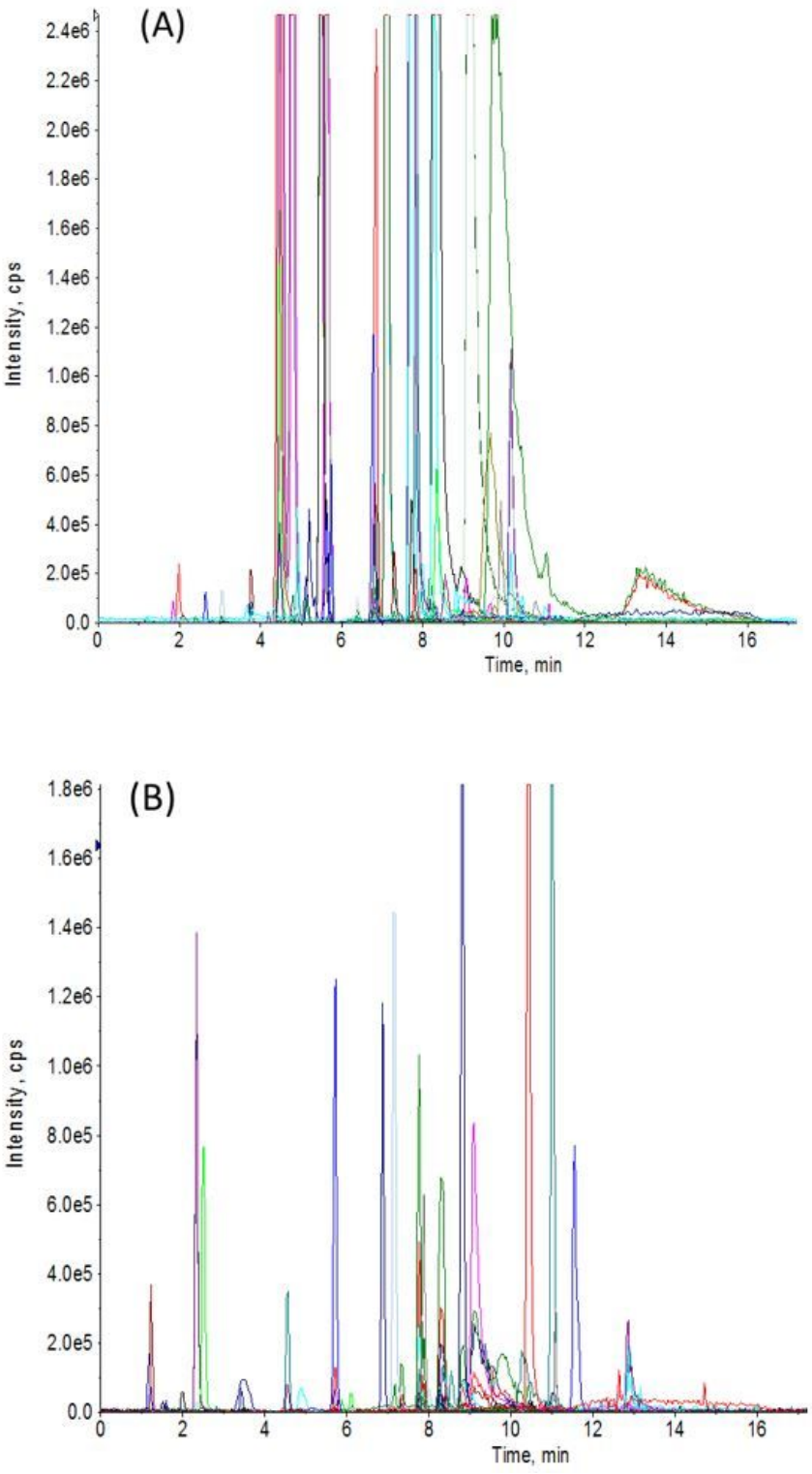

Figure 1

Representative MRM chromatograms of cell samples in the positive (A) and negative (B) detection modes.

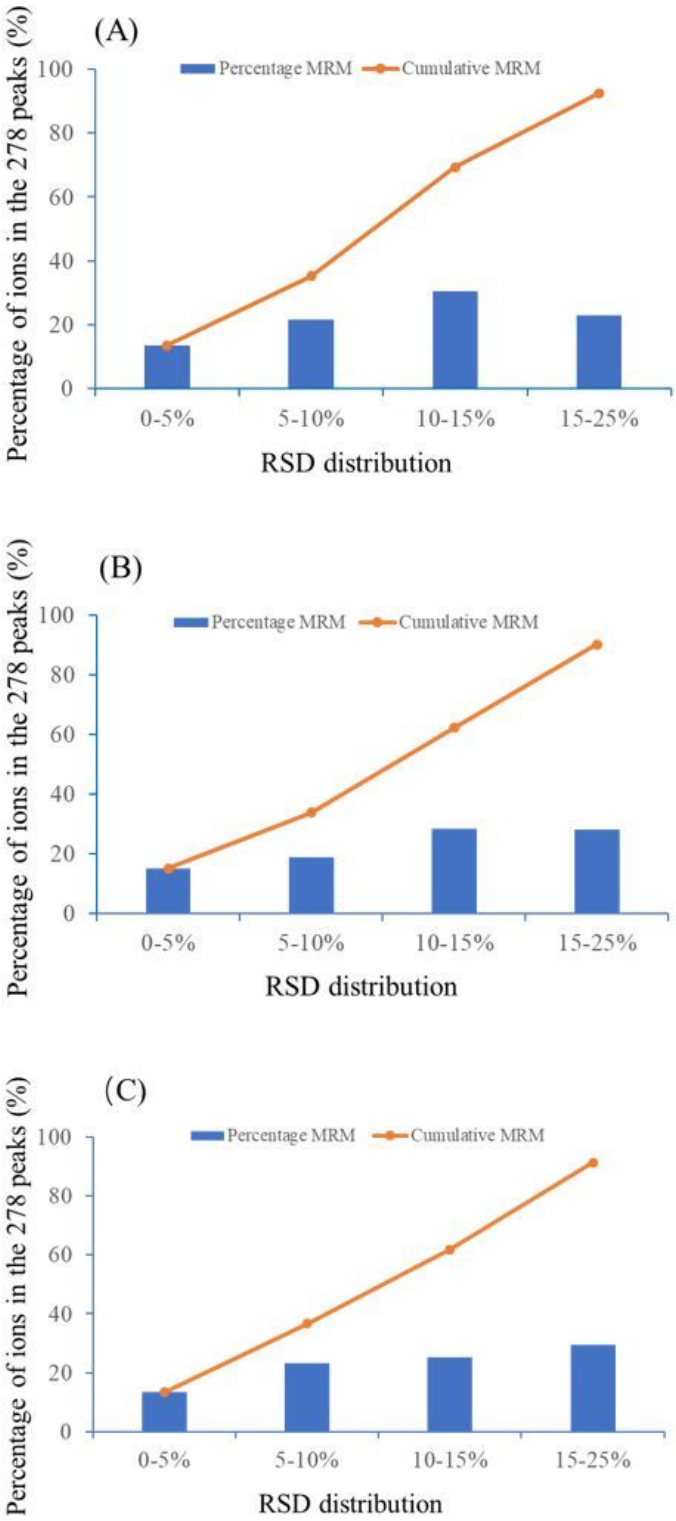

Figure 2

Intra-day precision (A), inter-day precision (B) and repeatability (C) of the 278 peaks detected by UHPLC-MS/MS.

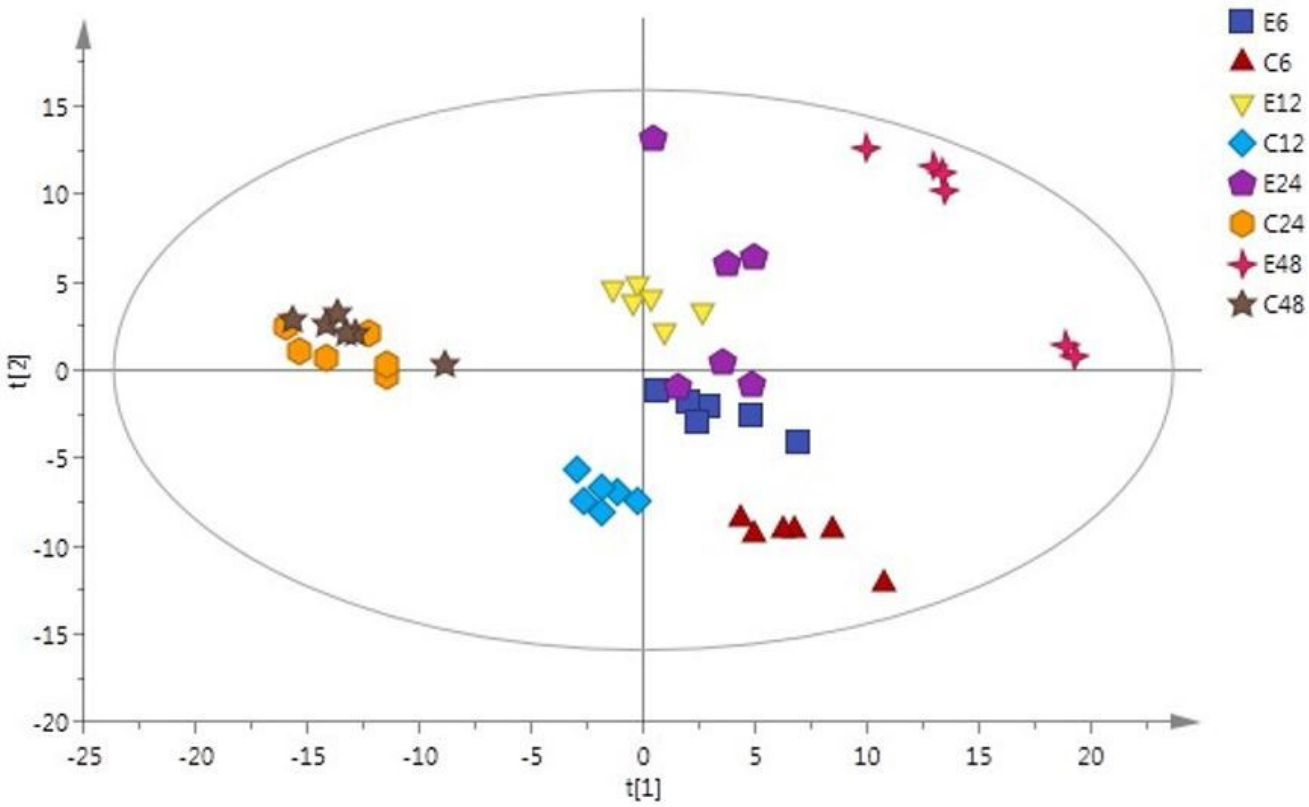

Figure 3

PCA-X score plot of erastin-treated MGC-803 cells and the controls.

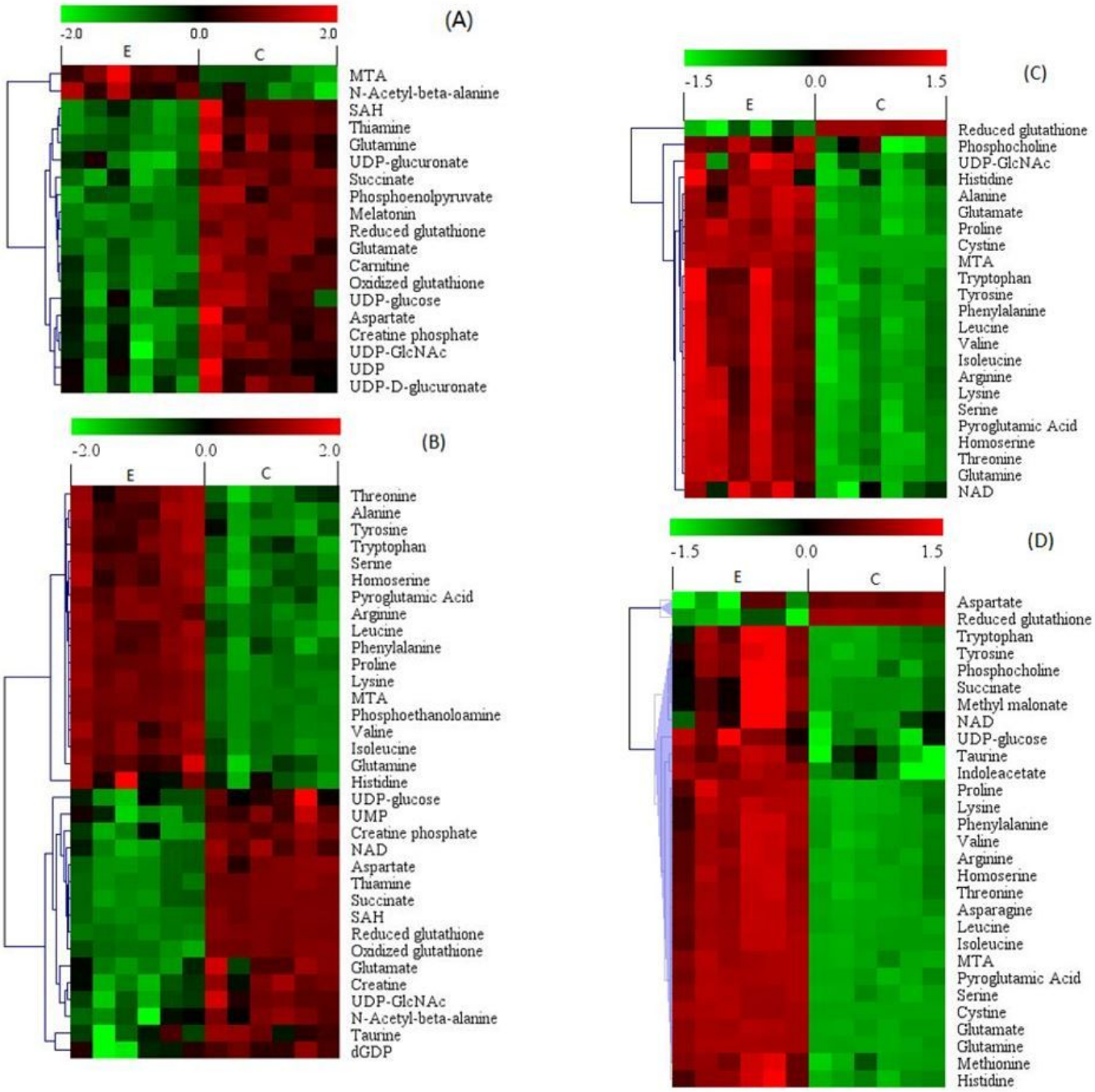

Figure 4

Heat map of differential metabolites generated by hierarchical Pearson clustering between erastin-treated MGC-803 cells and the controls: (A) 6h, (B) 12h, (C) 24h, (D) 48h. The dataset was screened using p-value < 0.05 and VIP > 1. Red color indicates an increased level of metabolites and green color indicates a decreased level of metabolites after erastin treatment, while black color means an equal level in four groups.

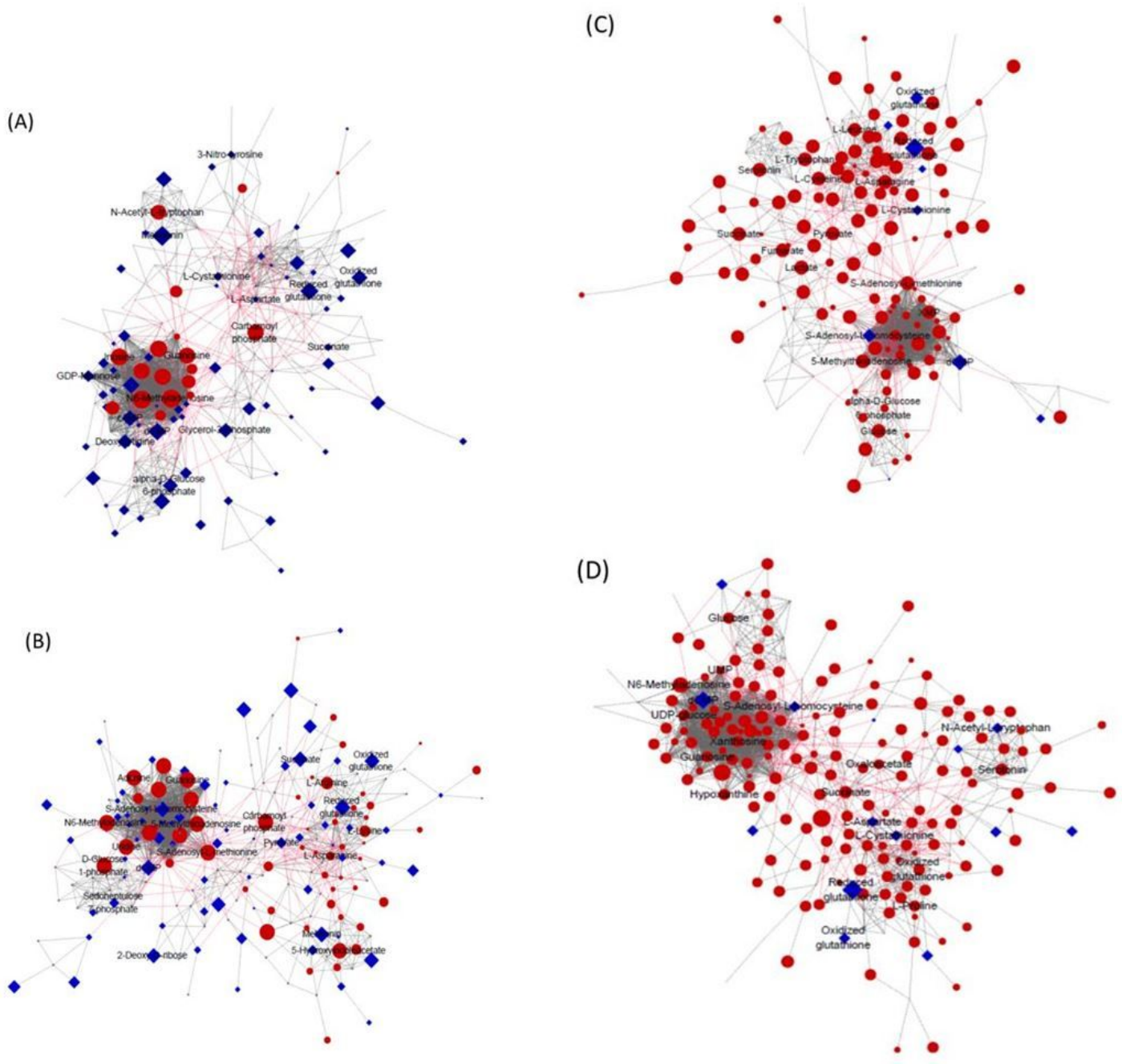

Figure 5

MetaMapp visualization of metabolomic data highlighting the differential metabolic regulation between the erastin-treated group and the controls: (A) 6 h, (B) 12 h, (C) 24 h, (D) 48 h. Red edges denote KEGG reactant pair links; grey edges symbolize Tanimoto chemical similarity at T > 700; unknowns are left out of these graphs for visual clarity. Metabolites found significantly up-regulated under exposure to erastin ($p < 0.05$) are given as red ball nodes; blue square nodes give down-regulated metabolites. Grey ball nodes reflect no significance.

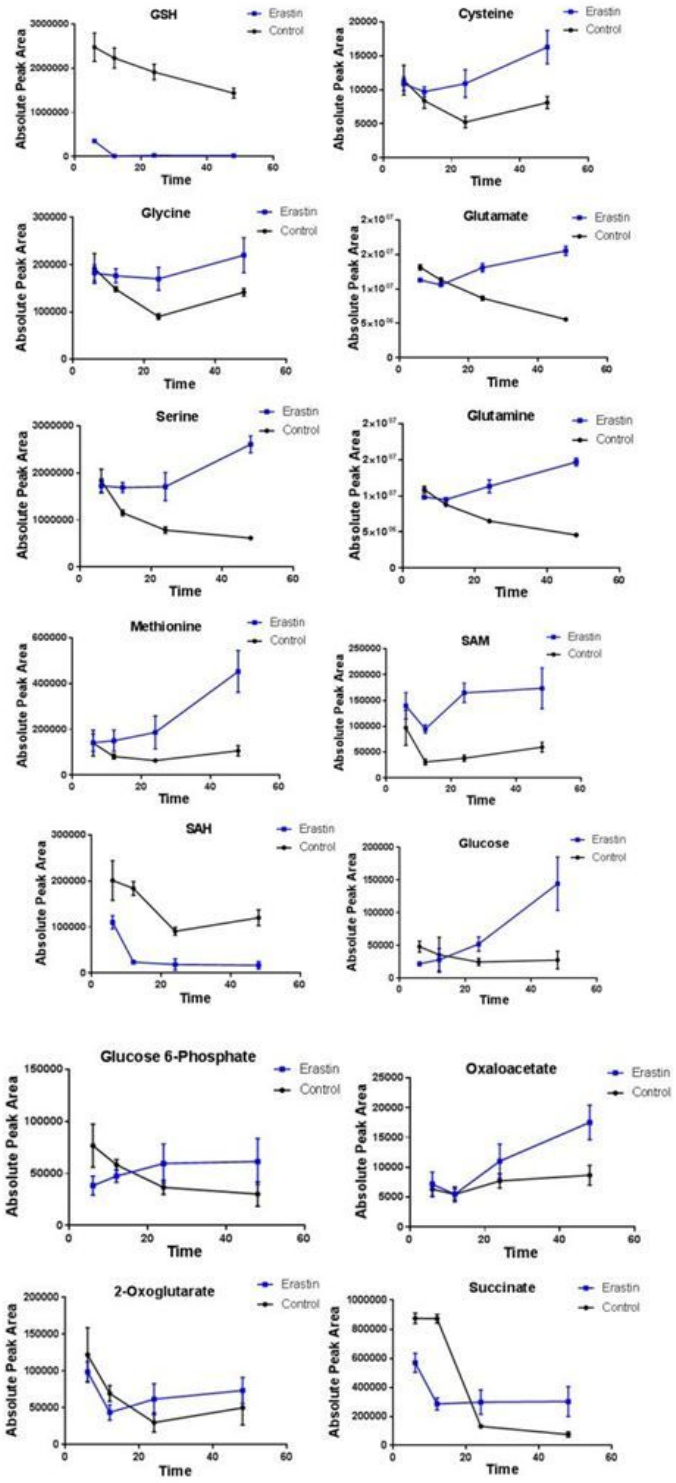

Figure 6

Response trajectory analysis of the metabolites in erastin-treated cells and the controls

Supplementary Files

This is a list of supplementary files associated with this preprint. Click to download.

- FigureS1.docx
- TableS1.xlsx
- TableS2.xlsx